Colloids and Surfaces B: Biointerfaces 232 (2023) 113587

Contents lists available at ScienceDirect

Colloids and Surfaces B: Biointerfaces

journal homepage: www.elsevier.com/locate/colsurfb

A biomimetic *in situ* mineralization ECM composite scaffold to promote endogenous bone regeneration

Lin Tang [a,1], Xiaoying Chen [a,1], Mei Wang [b], Yuhua Liu [a,*], Bowen Li [c], Yuke Li [a], Yi Zhang [d]

[a] *Department of Prosthodontics, Peking University School and Hospital of Stomatology & National Center of Stomatology & National Clinical Research Center for Oral Diseases & National Engineering Research Center of Oral Biomaterials and Digital Medical Devices & Beijing Key Laboratory of Digital Stomatology & National Health Commission Key Laboratory of Digital Technology of Stomatology, Beijing 100081, PR China*

[b] *Department of Stomatology, Beijing Chao-Yang Hospital, Capital Medical University, Beijing 100020, PR China*

[c] *Department of Stomatology, Beijing Hospital, National Center of Gerontology; Institute of Geriatric Medicine, Chinese Academy of Medical Sciences, Beijing 100730, PR China*

[d] *Department of General Dentistry II, Peking University School and Hospital of Stomatology & National Center of Stomatology & National Clinical Research Center for Oral Diseases & National Engineering Research Center of Oral Biomaterials and Digital Medical Devices & Beijing Key Laboratory of Digital Stomatology & National Health Commission Key Laboratory of Digital Technology of Stomatology, Beijing 100081, PR China*

ARTICLE INFO

Keywords:
Bone tissue engineering
Composite scaffold
Extracellular matrix
in situ mineralization
Small intestinal submucosa

ABSTRACT

Bone tissue engineering scaffolds constructed from single-component organic materials have inherent limitations. Inspired by the hierarchical structure of physiological natural bone hard tissues, our research explores the construction of organic-inorganic composite scaffold for bone regeneration. In this study, we used a natural and readily obtainable extracellular matrix (ECM) material, *i.e.*, decellularized small intestinal submucosa (SIS), to build the organic component of a phosphorylated hydroxyapatite nanocrystal-containing composite scaffold (nHA@SIS). Guided by polymer-induced liquid-precursor theory, we introduced a soluble inorganic mineralization solution to achieve an inorganic component of nHA@SIS. Using *in situ* mineralization, we successfully formed inorganic component within SIS and constructed nHA@SIS composite scaffold. We analyzed the physicochemical properties and the osteogenic role of nHA@SIS *via* a series of *in vitro* and *in vivo* studies. Compared with SIS scaffold, the nHA@SIS possessed suitable physicochemical properties, maintained the excellent cell activity of SIS and better guided reorganization of the cell skeleton, thereby achieving superior osteoconductivity and maintaining osteoinductivity at the protein and gene levels. Furthermore, the rat cranial defect area in the nHA@SIS scaffold group was mostly repaired after 12 weeks of implantation, with a larger amount of higher-density new bone tissue being visible at the edge and center than SIS and blank control group. This significantly improved *in vivo* osteogenic ability indicated the great potential of nHA@SIS for bone tissue engineering applications.

1. Introduction

Bone is primarily composed of type I collagen fibers (organic material) and phosphorylated hydroxyapatite nanocrystals (nHA) (inorganic material) embedded in the interstitial spaces of the fibers. The nHA deposits are located at the gaps in collagen fibers, forming a staggered pattern of intra- and extra-fibrous mineralization [1,2]. The deposition ratio of inorganic HAp in bone tissue is as high as 65% (mostly as extra-fiber mineral), with a small amount of intra-fiber mineral crystals arranged in a periodic array. Mineralized collagen fibers formed by the uniform distribution of nHA in collagen fibers are an important step in the development of bone tissue from micro to macro structures and have significant implications for the mechanical properties of bone. Better understanding the hierarchical levels of bone has led to the construction of high-performance organic-inorganic composite scaffolds, which are currently of intense interest for bone tissue engineering.

Organic materials for composite scaffold construction can be divided into synthetic polymers and natural polymers [3,4]. Among them, natural polymer materials have certain biological activity and good biocompatibility. Commonly used natural polymer materials include

* Corresponding author.
E-mail address: liuyuhua@bjmu.edu.cn (Y. Liu).
[1] These two authors contributed equally to this research

https://doi.org/10.1016/j.colsurfb.2023.113587
Received 7 June 2023; Received in revised form 4 October 2023; Accepted 10 October 2023
Available online 11 October 2023

collagen, chitosan, *etc.* [5,6]. In recent years, decellularized extracellular matrix (ECM) materials have attracted extensive attention of many researchers due to their unique composition and structural advantages. They retain biologically active components that play an important role in the process of biological induction and tissue remodeling with immunogenicity removal. Decellularized porcine small intestinal submucosa (SIS) is an ECM-derived matrix. In addition to the main component collagen, it is rich in endogenous growth factors such as vascular endothelial growth factor and epidermal growth factor and glycosaminoglycans. Its potential applications in cardiovascular, skin, other soft tissue defects, and bone regeneration have received widespread attention [7–9]. Decellularized small intestine submucosa (SIS) is a material derived from extracellular matrix. Our research group previously independently prepared decellularized SIS and reshaped it into a three-dimensional (3D) sponge scaffold that displayed improved osteogenic and angiogenic characteristics. However, the single-organic component scaffold had limitations including poor mechanical strength, rapid degradation, and asynchrony with the cycle of new bone formation; moreover, its functions and effects were limited [10–13].

Regarding inorganic materials for composite stents, they typically provide sufficient rigidity and a favorable microenvironment for bone formation in the biological scaffold. Commonly used inorganic materials include calcium phosphate ceramics, bioactive glass, calcium silicate, *etc.* [14]. Among them, hydroxyapatite (HA) is the main inorganic component of human and animal bones, participating in *in vivo* metabolism, and promoting the repair of defective tissues, with both osteoconductive and osteoinductive properties [15]. It not only provides a structural basis for the rigid function of bone tissue but also initiates many cell signaling pathways in bone regeneration. Therefore, HA has been widely used in bone and tooth restoration in biopolymer composites. However, single inorganic component scaffolds have common problems such as high material brittleness and fast release rate, and the osteogenic effect of HA in the process of bone repair is limited [11, 16–18]. A large number of studies have confirmed that the biological functions and physicochemical properties of HA can be chemically modified. It itself and its derivatives are often used as carriers of osteoblast-related cells and factors or used in combination with other biomaterials (such as collagen, chitosan, fibrin, and PCL, *etc.*) for bone regeneration [19–22].

There are various methods for adding inorganic materials into organic-inorganic composite scaffolds. One approach relies on direct mineral addition where minerals (such as HA particles) are directly added to the organic component solution, through different shaping methods *via* electrospinning [23,24], freeze-drying, or surface coating (*e.g.*, plasma spraying) [25]. Previous studies have successfully improved the mechanical properties of scaffolds by directly mixing HA nanoparticles with SIS solution and then freeze-drying to obtain composite scaffolds [26]. This method is often difficult for HA particle molecules to penetrate into the interior of organic fibers, and the mineralization is concentrated on the surface of the fiber. The other methods include *in situ* mineralization, wherein soluble calcium and phosphate ions are added to the organic solution system or a prefabricated organic scaffold is immersed in a solution containing the two mineral ions to form minerals in the organic component. Taking the self-assembled *in situ* mineralization as an example, mineral ions enter the internal gap of the fiber under the guidance of the polymer, and gradually deposit on the surface of the organic component fiber automatically, which can realize uniform layered intra- or extra-fibrous mineralization of an organic matrix [27,28].

Based on physiological endogenous mineralization in natural bone tissue, and considering by the following points: 1) the unique composition and structural advantages of SIS materials, including natural active ingredients such as collagen, glycosaminoglycans, and growth factors with biological induction and tissue remodeling effects, and our successful preparation and screening of the optimal ratio of SIS sponge-like scaffolds previously; 2) considering the inherent problems of single-component scaffolds; 3) among the different ways of inorganic-organic interactions, *in situ* mineralization method can achieve a structure more similar to natural bone tissue. In this study, the characteristics of the many negatively charged sites of collagen present in SIS were exploited as a template to introduce it into a mineralization fluid containing metal cations (inorganic components). According to the polymer-induced liquid precursor (PILP) process, a non-collagen protein mimetic (polyaspartic acid/poly acrylic acid; PASP/PAA) was synthesized [29]. nHA minerals were obtained *via* "bottom-up" *in situ* intra- and extra-fiber mineralization [27], completing the co-assembly of nHA minerals with SIS-ECM, establishing the combination of organic matter (collagen) toughness and inorganic matter (HA) rigidity, and ultimately achieving the construction of a uniformly distributed organic-inorganic composite scaffold (nHA@SIS). Then the nHA@SIS potential application in bone tissue engineering was explored.

2. Materials and methods

2.1. Preparation of nHA@SIS composite scaffold

We prepared SIS scaffolds according to a previously established protocol [30], briefly, which involves obtaining fresh decellularized submucosa from porcine small intestine after a series of defatting and decellularization processes, followed by preparation of freeze-dried powder. The powder was then dissolved in acetic acid and pepsin, molded, and then subjected to a second round of freeze-drying to obtain the organic component (SIS) of the nHA@SIS scaffold. The preparation of CaP_PILP solution was conducted according to previously reported methods [31]. In short, a calcium solution containing PASP was mixed with a phosphate solution containing PAA/PASP, and the pH was adjusted to 7.4 to obtain the final soluble bio-mineralization solution for providing the inorganic component of nHA@SIS. The *in situ* mineralization strategy involved adding a sufficient amount of mineralization solution to a well plate, completely submerging the pure organic component SIS sponge scaffold (37 °C, 50 rpm), and replace the mineralization solution every 2–3 days for a total of 14 days. The final nHA@SIS scaffold was obtained by freeze-drying for ready-to-use.

2.2. Physicochemical characterization of the nHA@SIS composite scaffold

2.2.1. Morphology and structure observation

Environmental scanning electron microscopy (ESEM) (Quanta 200F; FEI, Hillsboro, OR, USA) was used to observe the microstructure, pore size, and shape of the two scaffolds. ESEM images were processed using ImageJ software.

2.2.2. Energy Dispersive X-ray spectroscopy

Energy Dispersive X-ray Spectroscopy (EDS) mapping (ZEISS Gemini SEM 300, Germany) was performed to scan the surface of scaffolds and determine the chemical element (C, O, N, Ca, P) composition of the samples. The accelerated voltage was 15 kV and the detector was SE2 secondary electronic detector.

2.2.3. Porosity measurement

The porosity of the scaffold was determined using the liquid displacement method. Briefly, scaffold samples (n = 5) were soaked in anhydrous ethanol of known volume (V_0) for 10 min until saturated, and the residual volume after immersing the samples was recorded as V_1. After removing the scaffold, the remaining volume of ethanol was recorded as V_2. The porosity (P) of the scaffold was calculated as follows: $P\ (\%) = (V_0\text{-}V_2)/(V_1\text{-}V_2) * 100\%$.

2.2.4. Swelling ratio

After weighing (baseline weight = m_0), scaffold samples (n = 5) were placed in distilled water at room temperature. After 2 h, the scaffold was

removed from the water, and excess liquid was gently wiped away with a tissue. The weight of the sample was then measured (m_1). The swelling ratio (W) was calculated as follows: W (%) = (m_1-m_0)/m_0 * 100%.

2.2.5. In vitro degradation/dissolution rate

Scaffold samples were weighed as m_0, immersed in a centrifuge tube containing 20 mL of PBS buffer, and placed on a tabletop shaking incubator (37 °C, 80 rpm) for one day, with buffer replacement every other day. The samples were taken out on day 1, 3, 7, 14, and 21 respectively, washed and then freeze-dried and weighed as m_n. The dissolution rate (D) was calculated using the following formula: D (%) = (m_0-m_n)/m_0 * 100%.

2.2.6. Fourier transform infrared (FTIR) spectroscopy

The composition of SIS and nHA@SIS scaffolds was characterized using Fourier transform infrared (FTIR) spectroscopy (Bruker, USA).

2.2.7. Mechanical evaluation (compression modulus)

Scaffolds were prepared as cylindrical samples with a height of 8 mm and a diameter of 6 mm and compressed using a universal testing machine (Instron, USA). The compression modulus Ec (kPa) of the scaffold was calculated from the slope of the linear region of the stress-strain curve.

2.2.8. Protein adsorption

Bovine serum albumin (BSA) was used as a model protein. Samples (n = 5) were immersed in PBS solution containing BSA (2 mg/mL) at room temperature for 24 h. After removing the samples, the remaining protein solution was recovered and the absorbance at 570 nm was measured using a BCA assay kit in an ELISA reader (ELX800, Biotek, USA). The weight of the BSA protein captured by the scaffold was calculated based on the initial concentration of BSA and a standard curve.

2.2.9. Thermal stability analysis

The scaffold was analyzed by DTG and TGA analysis using a thermal gravimetric analyzer (Netzsch sta 449, Germany) in F3/F5 mode. The relationship between the mass and temperature changes of each group under program-controlled temperature was detected to analyze the decomposition and denaturation temperature and the loss of mass with the temperature of the scaffolds.

2.2.10. X-ray photoelectron spectroscopy (XPS)

X-ray photoelectron spectroscopy (Thermo escalab 250Xi, USA) was used to analyze the scaffold to detect the presence of calcium and phosphorus on the surface of the sample and to quantitatively determine the element content.

2.2.11. X-ray diffraction (XRD)

The scaffolds were analyzed using X-ray diffraction (Brucker D8 Advance, Germany) to characterize the inorganic components and phases of the analysis sample and perform quantitative measurements.

2.2.12. Inductively coupled plasma-optical emission spectrometry (ICP-OES)

The scaffolds were analyzed using inductively coupled plasma-optical emission spectrometry (ICP-OES) (Agilent ICPOES730, USA) to detect the concentration of calcium and phosphorus elements in the sample.

2.3. In vitro cell biology evaluation

2.3.1. Cell culture

Human bone marrow mesenchymal stem cells (hBMSCs) were isolated from volunteers' alveolar crest using the method described previously [32]. The study protocol followed the ethical principles and requirements of the Ethics Committee of Peking University School and Hospital of Stomatology. The hBMSCs were cultured in α-minimum essential medium (Gibco, USA) containing 10% fetal bovine serum (Hyclone, USA) and antibiotics (100 mg/mL streptomycin, 100 U/mL penicillin; Hyclone, USA) at 37 °C in a humidified atmosphere containing 5% CO2. The culture medium was changed every day. Passage 4–6 hBMSCs were used for the following experiments after digestion with 0.25% trypsin and suspension in a fresh culture medium [30].

2.3.2. Cell proliferation

hBMSCs were seeded onto two groups of scaffolds at a density of 2×10^4 per well, and the medium was changed every other day. Cell proliferation was evaluated using the CCK-8 assay kit (Donjindo, Japan) at day 0, 1, 3, 5, 7, 9, and 11 after seeding. The absorbance at 450 nm was measured using an ELISA reader (ELX800, Biotek, USA).

2.3.3. Cell viability

The effect of scaffolds on cell survival was studied using the LIVE/DEAD assay kit (KeyGEN BioTECH, China). The samples were washed with PBS and then stained for 30 min in a solution containing calcein AM and ethidium homodimer-1. After washing again with PBS, the samples were observed under a confocal laser scanning microscope (TCS SP8 X, Leica, Germany). Healthy cells fluoresce in green, while dead cell nuclei fluoresce in red [33].

2.3.4. Cell adhesion

hBMSCs were seeded onto two groups of sterilized scaffolds at a density of 2×10^4 per well. After 3 days of culture, the cells were fixed with 4% paraformaldehyde, stained for the cytoskeleton with FITC-phalloidin, and stained for the nuclei with DAPI. The cell spreading and adhesion were observed under a confocal laser scanning microscope (TCS SP8 X, Leica, Germany).

2.3.5. Alkaline phosphatase (ALP) staining and activity assay

hBMSCs were seeded onto two groups of scaffolds at a density of 2×10^4 per well, and after 3 days of culture, osteogenic induction was performed (100 nM dexamethasone, 50 μg/mL ascorbic acid, and 10 mM β-glycerophosphate). On day 7 and 14 of induction, the ALP staining kit (Cwbiotech, China) was used for staining, and observed under an inverted microscope (IX73, Olympus, Japan). The ALP activity in the samples was quantitatively determined using a protein detection kit (Cwbiotech, China) and an ALP activity assay kit (Jiancheng, China). The OD value of each sample was measured using an ELISA reader at 520 nm, and the ALP activity was calculated (U/gprot).

2.3.6. Alizarin Red S (ARS) Staining and Activity Quantification

hBMSCs were seeded onto two groups of scaffolds at a density of 2×10^4 cells per well. After 21 days of osteogenic induction, calcium nodules in the samples were observed by Alizarin Red S staining. The OD values at 562 nm were determined using a microplate reader after dissolving the nodules in 1% hexadecylpyridinium chloride (Sigma-Aldrich, USA).

2.3.7. Quantitative Real-Time PCR (qRT-PCR)

hBMSCs were seeded onto two groups of scaffolds at a density of 1×10^5 cells per well. After 7 and 14 days of osteogenic induction, total RNA was extracted from hBMSCs using Trizol reagent. Reverse transcription was performed using SYBR Green (Roche, Switzerland), and real-time PCR was performed using a real-time PCR instrument (7500, Applied Biosystems, USA) to detect the expression of osteogenic-related genes, including *ALP*, *BMP-2*, *COL-1*, *OSX*, *OPN*, *RUNX-2 and SMAD1*. The primers synthesized were as follows: *Human-GAPDH*, GGAGCGAGATCCCTCCAAAAT and GGCTGTTGTCATACTTC-TCATGG; *Human-ALP*, CTATCCTGGCTCCGTG and GCTGGCA-GTGGTCAGA; *Human-BMP-2*, TGACGAGGTCCTGAGCGAGTTC and TGAGTGCCTGCGATACAGGTCTAG; *Human-COL-1*, AGAGGAAGGAAAGCGAGGAG and

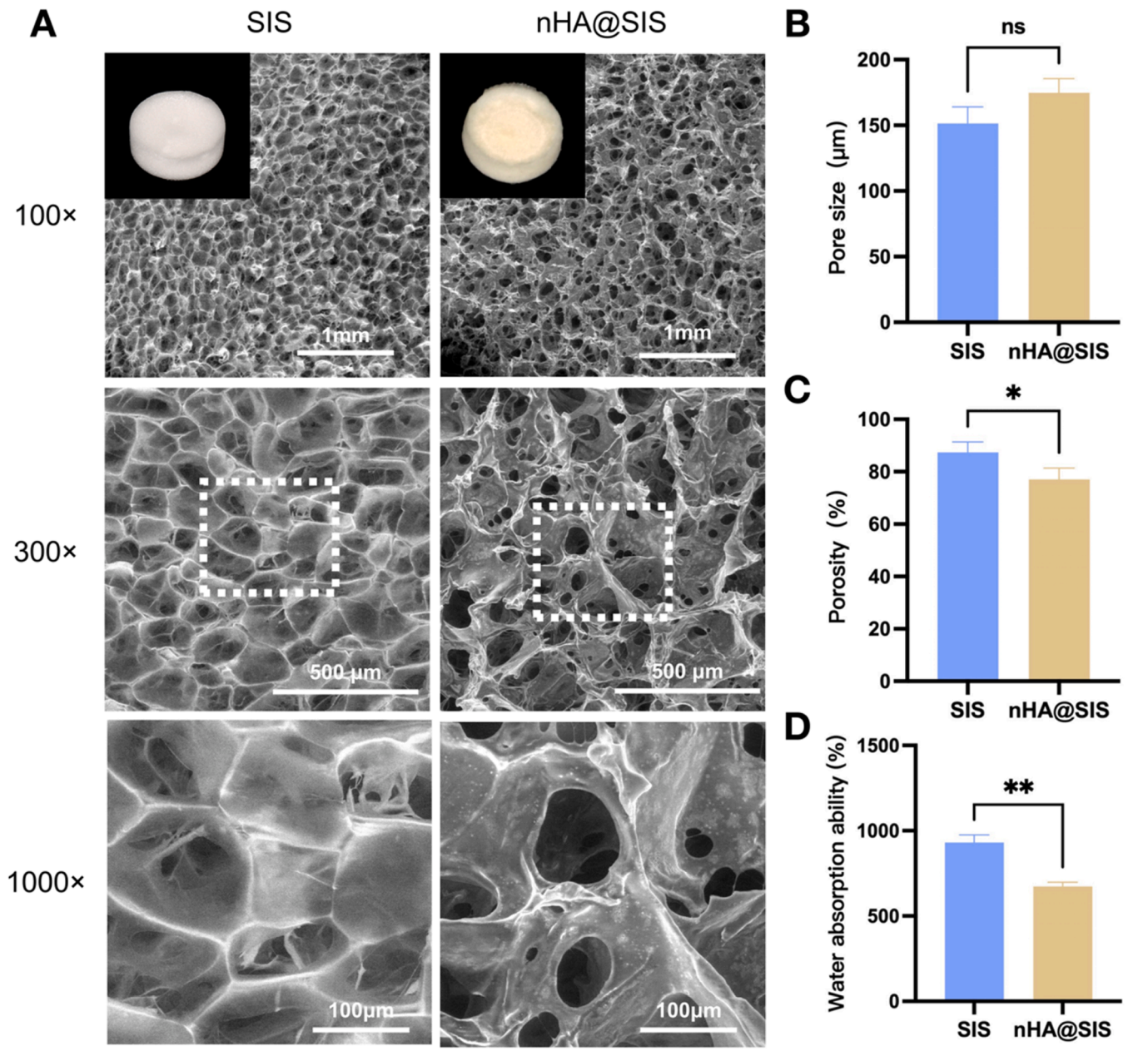

Fig. 1. Characteristics of SIS and nHA@SIS scaffolds. (A) Overview and ESEM images (100 ×,300 ×,1000 ×). (B) Pore size. (C) Porosity. (D) Water absorption ability. * , $P < 0.05$.

GGACCAGCAACACCATCTG; *Human-OSX*, AGCAGCAGTAGCAGAAGCA and CAGCAGTCCC-ATAGGCATC; *Human-RUNX-2*, CACTGGCGCTG-CAACAAGA and CATTCCGGAGCTCAGCAGAATAA; *Human-OPN*, CC ATGGAACTTGGACTTT-CTTGG and GAGCTCTTAATGATGGTGATGG TGGTGAT-GATG; and *Human-SMAD1*, AGATGTTCAGGCGGTTGCT-TAT and AGGCAT-GGAACGCTTCACC. The mRNA expression levels of all genes were normalized to the internal control *GAPDH*. Relative expression was calculated using the $2^{-\Delta\Delta CT}$ method [34].

2.4. In vivo osteogenic evaluation

2.4.1. Animal model

All animal surgical procedures were approved by the Animal Research Committee of Peking University Health Science Center. SPF grade SD rats (male, aged 6–8 weeks, weighing 300–350 g) were randomly divided into three groups: blank control group, SIS scaffold or nHA@SIS scaffold implantation group. Under pentobarbital sodium (50 mg/kg) anesthesia, a circular bone defect with a diameter of 5 mm was created on both sides of the rat's skull using an implant machine, and the surgical area was cooled with saline during the procedure. Different scaffolds were placed in the defect area, while the skull defect without a scaffold was used as the blank control group. After 12 weeks, the rats were sacrificed, and the skulls were harvested for further analysis.

2.4.2. Micro-CT analysis

Computer tomography (micro-CT, Bruker, Belgium) was used for reconstruction and data analysis using CT analysis software Acquisition Workplace and Inveon Research Workplace software [30]. The bone mineral density (BMD) and bone volume fraction (bone volume/total volume, BV/TV) as well as the trabecular thickness (Tb.Th (mm)), the trabecular number (Tb.N (1/mm)), the trabecular Spacing (Tb.Sp (mm)) of the newly formed bone were calculated and analyzed.

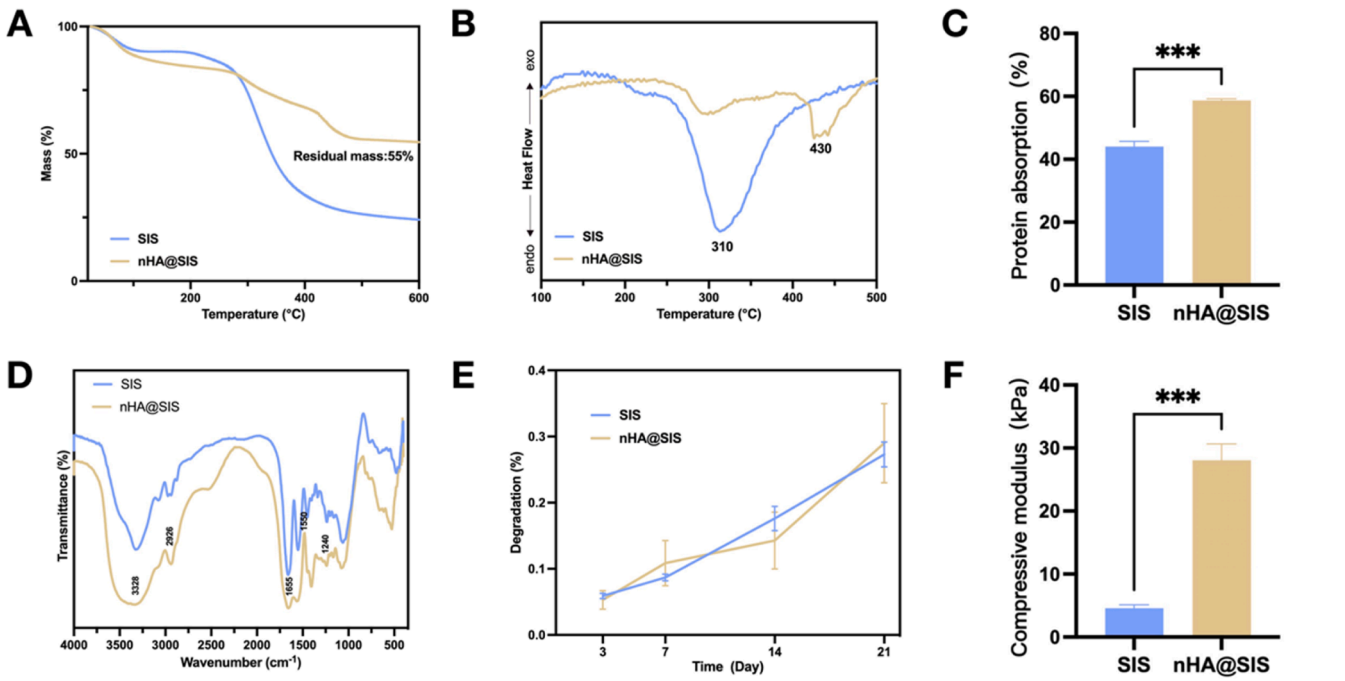

Fig. 2. Analysis of Physicochemical properties. (A) TGA. (B) DTG. (C) Protein absorption. (D) FTIR. (E)Degradation of PBS. (F) Compressive modulus. * , $P < 0.05$.

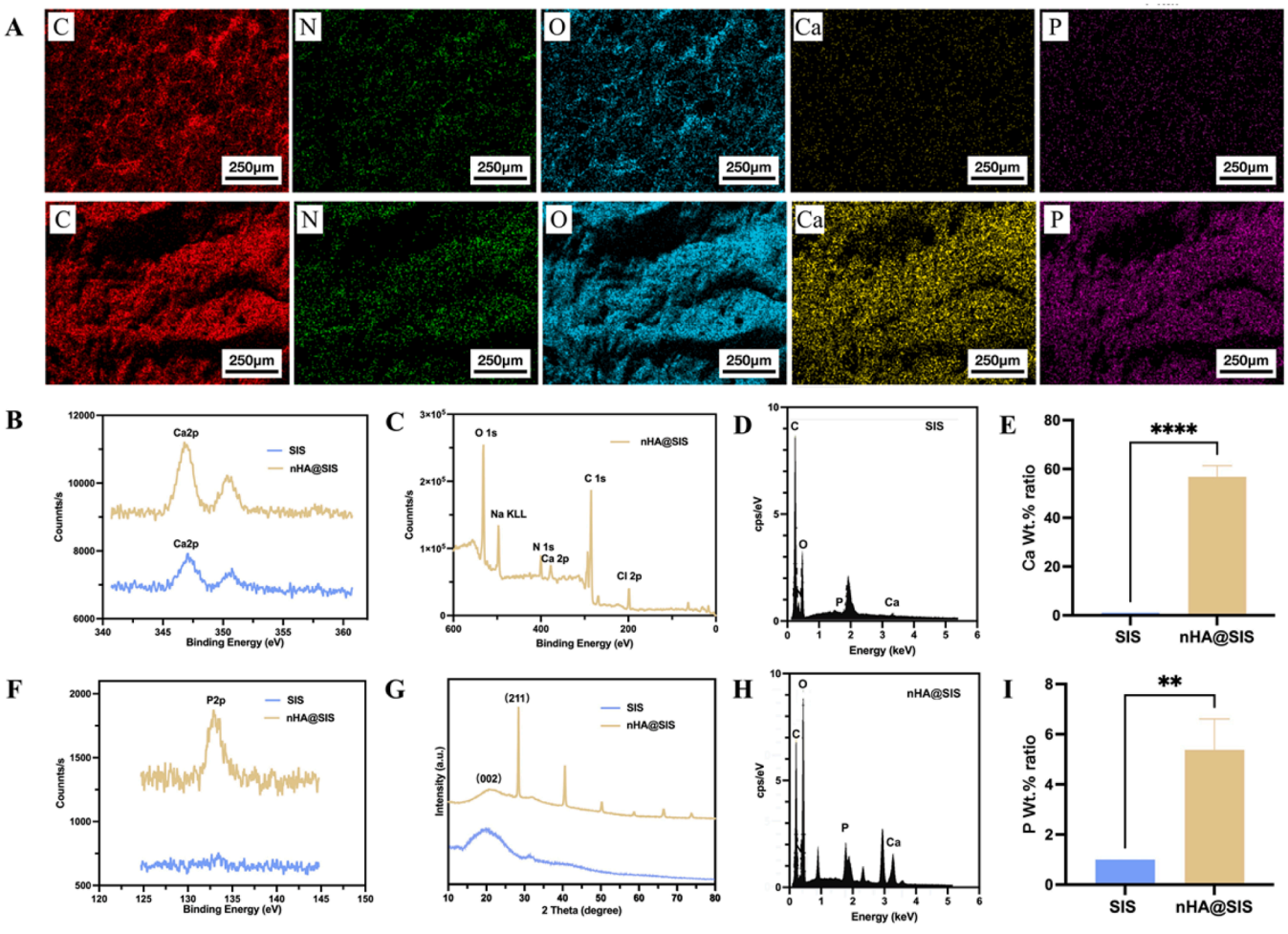

Fig. 3. Mineralization analysis of scaffolds. (A, D, H) EDS mapping. (B, F) XPS. (C, G) XRD. (E, I) ICP. * , $P < 0.05$.

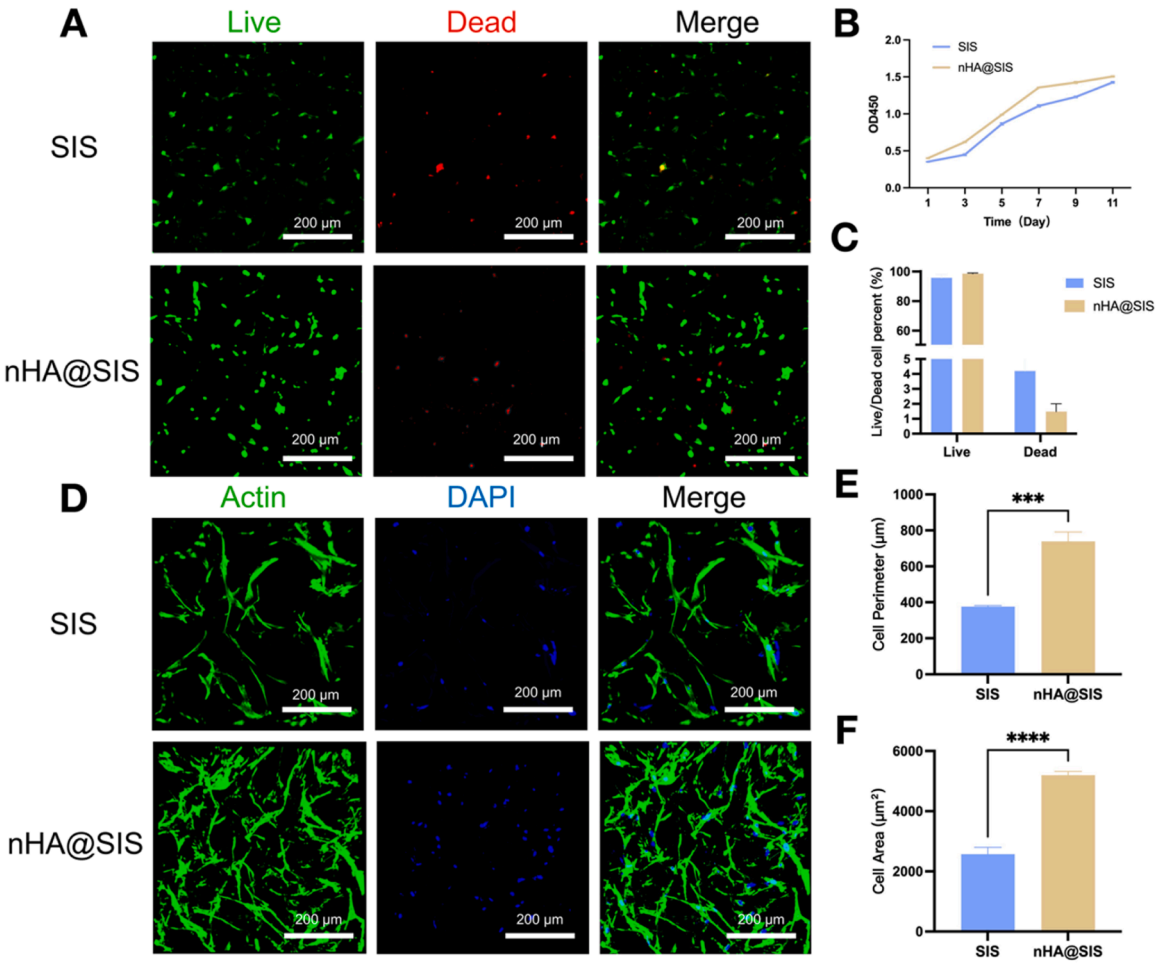

Fig. 4. Biocompatibility of the scaffolds. (A) Live/dead cell staining. (B) CCK-8 cell proliferation assay. (C) Live/dead cell percent. (D) Actin/DAPI staining. (E) Cell Perimeter. (F) Cell area. * , $P < 0.05$.

2.4.3. *Histological staining*

After micro-CT scanning, the samples were decalcified, paraffin-embedded, and sectioned (5 μm). Haematoxylin and eosin (HE), Masson's trichrome, and a two-step detection kit (Zhongshan Golden Bridge Biotechnology, China) were used for histological staining and observation.

2.5. *Statistical analysis*

Statistical analysis was performed using SPSS software version 23.0 (IBM, USA). Data were presented as mean ± standard deviation. Independent samples t-test was used to compare means between two groups. One-way ANOVA was used to compare means more than two groups, followed by post-hoc tests using Tukey or Dunnnett's method and Fisher's least significant difference test. $P < 0.05$ was considered to indicate statistical significance.

3. Results and discussion

In this study, to construct an nHA@SIS composite scaffold as a potential bone tissue engineering scaffold having good organic-inorganic interactions, 1% SIS was selected as the organic component, and CaP_-PILP mineralization solution as the soluble inorganic component, based on a previous study [31]. This approach leveraged the collagen-rich aspect of SIS, which has negatively charged components, and the *in situ* mineralization solution containing a large amount of positively charged soluble inorganic ions. The attraction between positive and negative charges, along with the introduction of PAA and PASP as non-collagen protein mimics, stabilized the mineralization solution and promoted the production of nHA, enabled uniformly distributed nHA deposition inside and outside the fibers, and ultimately provided the desired nHA@SIS scaffold.

Under the ESEM microscope, the two groups of scaffolds revealed a highly porous, interconnected and regular sponge-like structure.Thick collagen fibers and evenly deposited and uniformly arranged mineral crystals were observed inside the pores and on the surface of the fibers, and made the scaffold structure more compact. This microstructure can provide an optimized microenvironment for stem cell regulation, self-renewal, and multi-lineage differentiation potential [35,36]. The nHA@SIS scaffold had a good pore size (151.40 ± 12.77 μm), and although the pore ratio of the mineral crystal deposition was lower compared with that of the SIS scaffold, nHA@SIS can still provide sufficient space for cell attachment, which is of great significance for the growth of adhering cells and transport of metabolic waste [37]. Figs. 1–7.

The nHA@SIS scaffold was hydrophilic and had a moderate degradation rate and better protein adsorption capacity. During the first 7 days of phosphate-buffered saline (PBS) degradation, the slightly higher degradation ratio compared with SIS may be due to the release of some small, mineralized particles or rupture of the surface. Subsequently, the degradation of nHA@SIS gradually approached stability. Within the 21 days observation period, both scaffold groups showed a relatively stable degradation process and rate in PBS solution; the dissolution rate was around 30% on the 21st day. Fourier-transform infrared spectroscopy

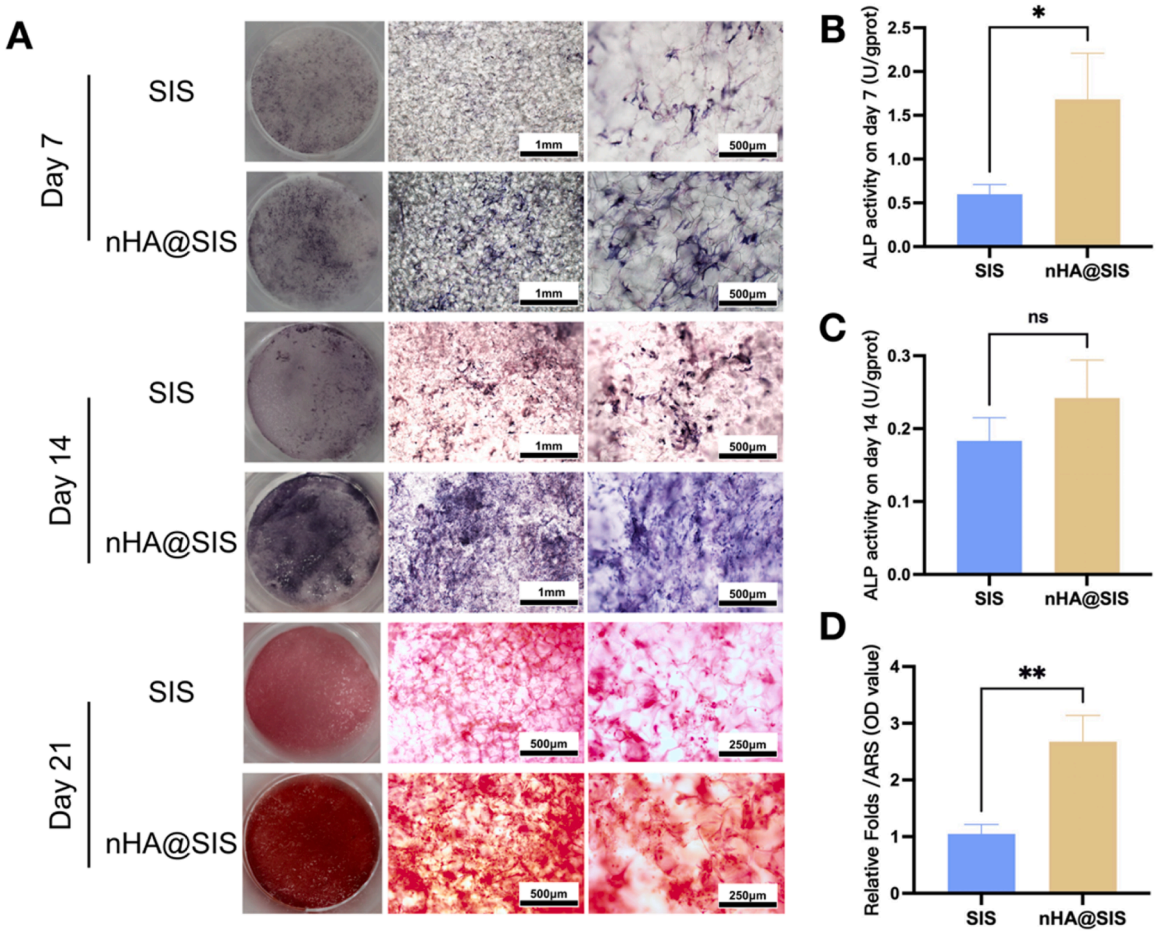

Fig. 5. Osteogenic differentiation of hBMSCs. (A) ALP and alizarin red S (ARS) staining. (B, C) Quantitative assessment of ALP activity. (D) Semi-quantitative assessment of ARS findings. * , $P < 0.05$.

confirmed the presence of phosphates, carbonates (replacing hydroxyl and phosphate groups in hydroxyapatite), acylamide I (1655 cm^{-1}) (C═O stretching vibration), acylamide II (1550 cm^{-1}) (N–H bending and C–N stretching vibration), and acylamide III (1240 cm^{-1}) (C–N stretching and N–H planar bending) in nHA@SIS, while the characteristic peak of acylamide B (2926 cm^{-1}) remained unchanged, suggesting that biomimetic mineralization did not alter the structure of collagen and maintained the good structural characteristics of SIS. The acylamide A spectral band (3328 cm^{-1}; N–H stretching vibration) of the nHA@SIS group was slightly broadened, possibly due to hydrogen bonding interactions between HAP and collagen.

One significant feature of the organic-inorganic composite scaffold is its improved mechanical strength compared with the biological scaffold. Scaffolds with appropriate mechanical properties can provide a reliable environment for cell adhesion and osteogenic differentiation. Previous studies have shown that some stiffer scaffolds can enhance osteogenic differentiation through integrin-mediated mechanical transduction [38–41]. Compared with the SIS scaffold (4.58 ± 0.53 kPa), the mechanical properties of the biomineralized nHA@SIS composite scaffold (28.07 ± 2.57 kPa) in this study were significantly enhanced by seven-to-eight times. This improvement is attributed to the good dispersion of nHA in the SIS, which enhanced the interfacial bonding strength and maximized the reinforcing effect of the organic-inorganic interfacial interactions. Subsequently, we observed further enhancement of the thermal stability of the nHA@SIS scaffold. Thermogravimetric analysis (TGA) confirmed significant mass attenuation of the SIS scaffold at 300 °C; this occurred at 350 °C for the nHA@SIS scaffold. The degree of mineralization of the collagen matrix was also determined using TGA. The mass attenuation between 300 and 450 °C was due to the loss of collagen protein chains and fragments, while that between 450 and 600 °C was due to the loss of organic residues. The residual mass after 600 °C corresponded to the inorganic material present after complete thermal degradation. The residual mass of nHA@SIS was about 55%, which is the proportion of HAp formed by mineralization and is very close to the proportion of HAp in natural bone tissue (60%) [42]. Differential TGA of nHA@SIS revealed two decomposition peaks. The second peak corresponded to the decomposition of organic components. The first peak occurred at 310 °C for the control group and 430 °C for nHA@SIS. This improved thermal stability of the composite scaffold was attributed to changes in the micro- and nanostructures.

Energy-dispersive spectra results confirmed that C, N, and O were present in the SIS and nHA@SIS scaffolds, and the characteristic peaks of Ca and P were detected in the nHA@SIS scaffold. The mapping elemental analysis also indicated that Ca and P were uniformly distributed in the nHA@SIS scaffold. X-ray photoelectron spectra revealed a significant increase in the Ca/P element concentration of the nHA@SIS composite scaffold. This ratio is an important characteristic of HAp, and the increased Ca/P concentration was consistent with the presence of more calcium phosphate crystals. Inductively coupled plasma-atomic emission spectroscopy confirmed that the Ca/P ratio (1.38 ± 0.10) was different from that of HAp, suggesting that HAp was not the only mineral phase present. The X-ray diffraction pattern of the scaffold displayed two strong reflections at $2\theta = 26°$ and 31.8° corresponding to the (002) and (211) planes of HAp, respectively. This was consistent with the ESEM observation of thickened collagen fibers and uniformly deposited mineral crystals in the nHA@SIS composite

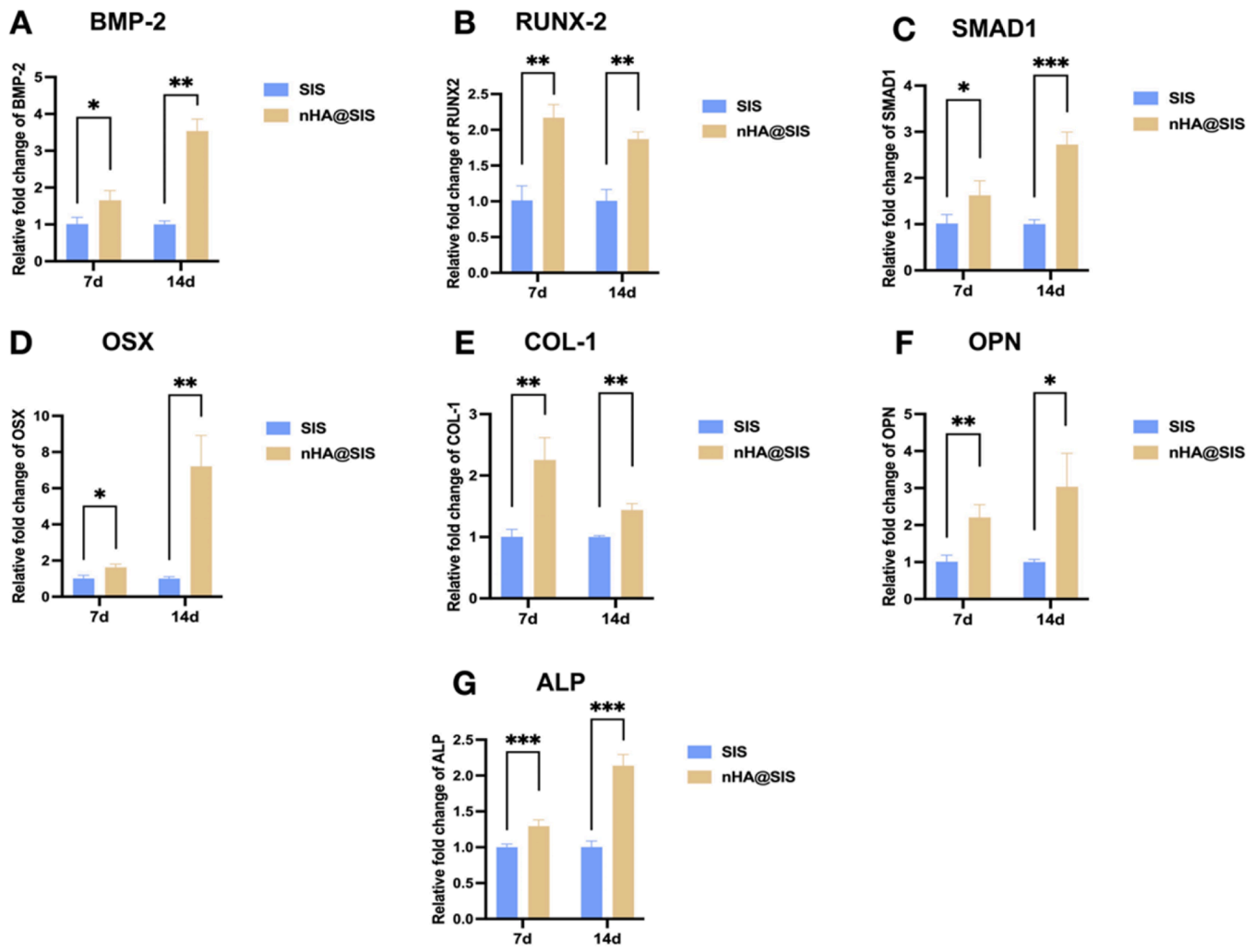

Fig. 6. Relative mRNA expression levels of (A) *BMP-2,* (B) *RUNX-2,* (C) *SMAD1,* (D) *OSX,* (E) *COL-1,* (F) *OPN,* (G) *ALP* on day 7 and 14 after *in vitro* osteogenic induction of hBMSCs. * , $P < 0.05$.

scaffold, which improved the mechanical and thermal stability. Deposition of these mineral crystals also provided sufficient space and protection to allow internal cells to resist pressure from the surrounding microenvironment, thereby improving cell survival.

Cell Counting Kit-8 and live/dead assays confirmed that nHA@SIS had better cell proliferation activity. As surface-dependent cells, firm and sufficient attachment of human bone marrow mesenchymal stem cells (hBMSCs) to the matrix at an early stage is a prerequisite for their further spread and migration [43]. This observation was further confirmed by double immunostaining for F-actin, which showed the cytoskeletal arrangements. After 72 h of cell seeding, more hBMSCs were well-attached to the scaffold surface and stretched into spindle-shaped cells with prominent filamentous and lamellipodial pseudopodia extending to the surface, and the cells were more closely aligned and interconnected in the nHA@SIS group. The quantitative data indicated that hBMSCs seeded on the nHA@SIS scaffold had greater cell area and more branch points. This may be related to the unique surface topography and chemical interfacial properties of nHA@SIS, which maintained the excellent biological properties of SIS while guiding rearrangement of the cell skeleton [43].

After hBMSCs were seeded on the nHA@SIS scaffold and induced to osteogenic differentiation, more mineralization nodules were formed in the early stage (day 7) of ALP staining and mid-to-late stage (day 21) of ARS staining, consistent with the microscopic and quantitative results. This indicated that the nHA@SIS scaffold provided better osteoconduction and maintained osteoinductivity [44–46]. These advantages might be related to the mechanical stimulation of nHA@SIS, which allowed cells to spread and attach more easily, and thus sense mechanical stimulation, thereby providing more differentiation opportunities. We further speculated that nHA@SIS may enhance *in vivo* osteogenic differentiation and accelerate bone mineralization by promoting calcium deposition [47]. This suggestion relates to the transformation of biomaterial scaffolds from structures with purely passive functions to structures with a series of regulatory functions based on the morphological, physical, and chemical properties of stem cells and the local microenvironment [48].

The nHA@SIS composite scaffold significantly increased the expression levels of *ALP*, *BMP-2*, *COL-1*, *OPN, RUNX-2, SMAD1* and *OSX* on day 7 and 14. These results suggest that nHA@SIS may promote osteogenic differentiation of BMSCs by activating *BMP-2 /SMAD1/ RUNX-2/Osterix* signaling pathway. Different from synthetic biomaterials, such as PLLA and PEEK, nHA@SIS containing decellularized ECM displayed the high-level simulation characteristics typical of a complex extracellular microenvironment, which regulates cell function and maintains and/or guides stem cell differentiation without stimulating the immune response of the host tissue, and provides the signals necessary to regulate cell function [46,49,50].

In situ tissue engineering was conducted to treat critical bone defects in rat skulls *in vivo* without exogenous cell introduction, thereby reducing the likelihood of low cell survival rates [51]. Mineralized

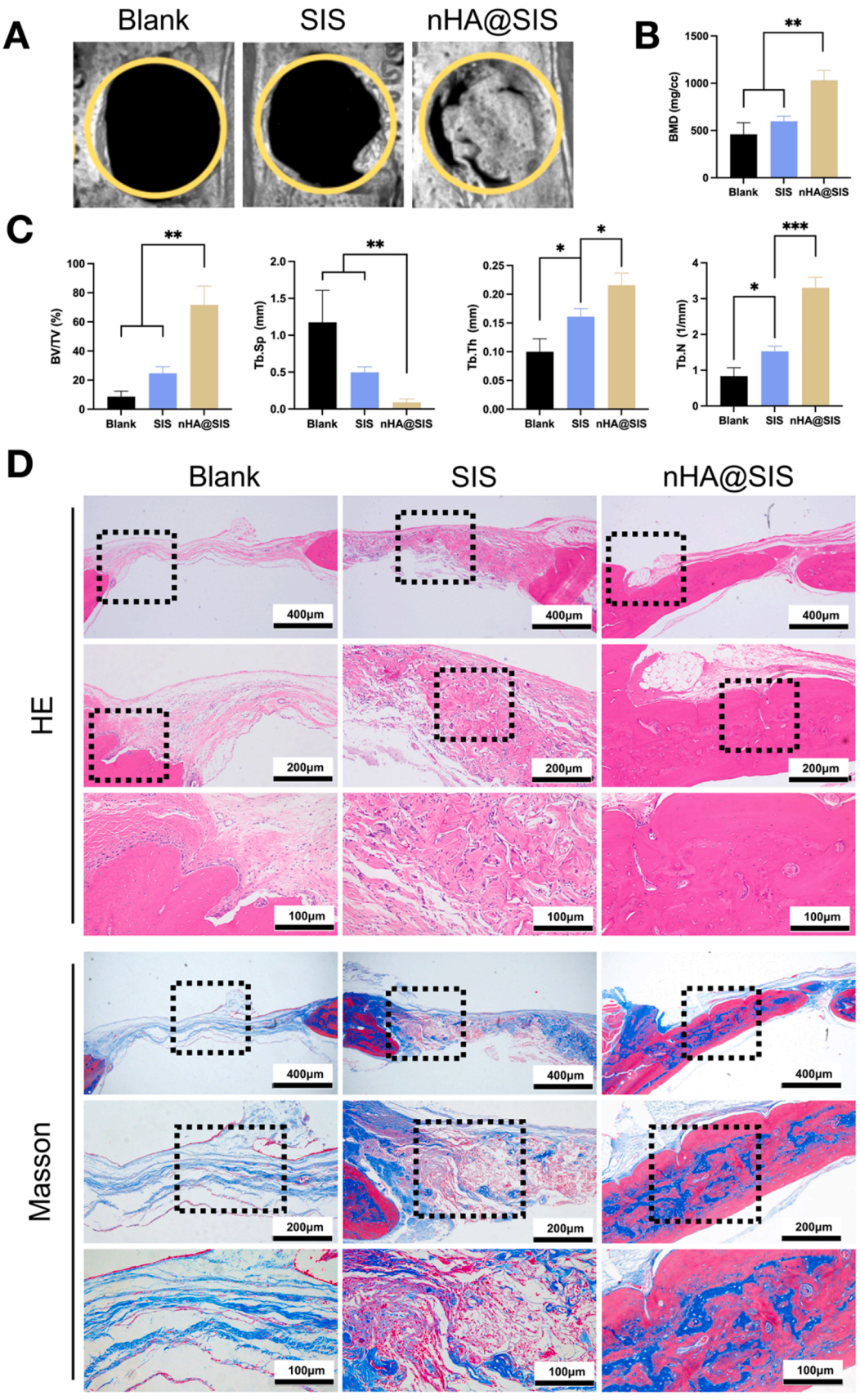

Fig. 7. Bone regeneration in critical-size calvarial defects. (A) Micro-CT. (B) BMD. (C) BV/TV, Tb. Sp, Tb.Th, Tb.N. (D) HE staining and Masson staining. * , $P < 0.05$.

scaffolds can provide the equivalent bone regeneration effect of ECM secreted *in vitro* and deposited on true bone ceramic scaffolds [52]. As expected, 3D reconstruction by microcomputed tomography confirmed almost no new bone tissue in the blank group after 12 weeks. This indicated that the rat skull tissue had little or no self-regeneration ability. In the nHA@SIS group, the bone defect area was largely repaired, with abundant high-density new bone tissue visible at the edge and center. The bone density was similar to that of the surrounding skull bone, and the density range was much larger than that of the SIS and blank groups. Bone volume fraction and bone mineral density were significantly increased, and histological staining confirmed large amounts of newly formed fibrous bone and blood vessels in the defect center. This might be related to the high release of calcium ions caused by nHA@SIS [53]. Hematoxylin and eosin and Masson staining results indicated that the nHA@SIS scaffold exhibited good tissue integration ability and significantly increased new bone-like tissue and enhanced osteoblast arrangement. Unlike in the SIS group, no incompletely degraded scaffold materials were found in mature bone islands of the nHA@SIS group, indicating that the composite scaffold played a role throughout the formation of new bone and gradually integrated with the surrounding tissue while degrading.

This behavior was closely related to the unique structure of the nHA@SIS scaffold; it contains natural SIS, which mimics the unique microenvironment of natural bone ECM, as well as uniformly distributed crystals formed by soluble minerals that have various structural, mechanical, and biological properties important for regulating stem cell fate. The homing and osteogenic differentiation of stem cells continuously occurred during the process of bone regeneration, and promoted the recruitment of endogenous mesenchymal stem cells to the injury site, further induced bone marrow stromal cell osteogenic differentiation, and displayed an appropriate degradation rate; thus providing space for new bone tissue to occupy and ultimately realize *in situ* bone regeneration without the need for exogenous cells.

4. Conclusion

In this study, based on the excellent biocompatibility of SIS, nHA@SIS was successfully constructed through *in situ* mineralization of CaP_PILP method. It has achieved nHA infiltration of collagen and uniform distribution, with good physical and chemical properties. Moreover, nHA@SIS could maintain the excellent biocompatibility of SIS, better guide the reorganization of the cytoskeleton, and effectively enhance the expression of osteogenic related genes. In the rat critical cranial defect model of nHA@SIS implantation group for 12 weeks, a larger amount of high-density new bone formation could be observed at the edge and center of the bone defect area, revealed better osteogenic performance. These indicated nHA@SIS might be a potential bone regeneration scaffold materials with promising application prospects.

Funding

This work was supported by the National Natural Science Foundation of China (Grant Nos. 81801027 (L.T.)).

CRediT authorship contribution statement

Lin Tang: Conceptualization, Methodology, Validation, Formal analysis, Resources, Writing - original draft, Writing - review & editing, Funding acquisition. **Xiaoying Chen:** Methodology, Validation, Formal analysis, Data curation, Writing - original draft. **Mei Wang:** Conceptualization, Data curation, Formal analysis. **Yuhua Liu:** Conceptualization, Supervision, Resources, Writing - review & editing, Funding acquisition. **Bowen Li:** Investigation, Formal analysis. **Yuke Li:** Investigation. **Yi Zhang:** Investigation.

Declaration of Competing Interest

The authors declare that they have no known competing financial interests or personal relationships that could have appeared to influence the work reported in this paper.

Data availability

Data will be made available on request.

Acknowledgements

We sincerely thank the faculty and staff from Biomechanics Research or Central Laboratory of Stomatology School and Hospital of Peking University for all support.

References

[1] A. Hasan, B. Byambaa, M. Morshed, M.I. Cheikh, R.A. Shakoor, T. Mustafy, H. E. Marei, Advances in osteobiologic materials for bone substitutes, J. Tissue Eng. Regen. Med 12 (2018) 1448–1468, https://doi.org/10.1002/term.2677.
[2] Z. Li, T. Du, C. Ruan, X. Niu, Bioinspired mineralized collagen scaffolds for bone tissue engineering, Bioact. Mater. 6 (2021) 1491–1511, https://doi.org/10.1016/j.bioactmat.2020.11.004.
[3] L. Zhang, G. Yang, B.N. Johnson, X. Jia, Three-dimensional (3D) printed scaffold and material selection for bone repair, Acta Biomater. 84 (2019) 16–33, https://doi.org/10.1016/j.actbio.2018.11.039.
[4] S.S. Preethi, M.A. Haritha, C.S. Viji, N. Selvamurugan, Bone tissue engineering: Scaffold spreparation using chitosan and other biomaterials with different design and fabrication techniques, Int. J. Biol. Macromol. 119 (2018) 1228–1239, https://doi.org/10.1016/j.ijbiomac.2018.08.056.
[5] E. Sayin, R.H. Rashid, J.C. Rodríguez-Cabello, A. Elsheikh, E.T. Baran, V. Hasirci, Human adipose derived stem cells are superior to human osteoblasts (HOB) in bone tissue engineering on a collagen-fibroin-ELR blend, Bioact. Mater. 2 (2017) 71–81, https://doi.org/10.1016/j.bioactmat.2017.04.001.
[6] J.I. Dawson, D.A. Wahl, S.A. Lanham, J.M. Kanczler, J.T. Czernuszka, R.O. Oreffo, Development of specific collagen scaffolds to support the osteogenicand chondrogenic differentiation of human bone marrow stromal cells, Biomaterials 29 (2008) 3105–3116, https://doi.org/10.1016/j.biomaterials.2008.03.040.
[7] M. Li, T. Zhang, J. Jiang, Y. Mao, A. Zhang, J. Zhao, ECM coating modi-fication generated by optimized decellularization process improves functional behavior of BMSCs, Mater. Sci. Eng.: C 105 (2019), 110039, https://doi.org/10.1016/j.msec.2019.110039.
[8] X.R. Zhang, Y.Z. Huang, H.W. Gao, Y.L. Jiang, J.G. Hu, J.K. Pi, A.J. Chen, Y. Zhang, L. Zhou, H.Q. Xie, Hypoxic preconditioning of human urine-derived stem cell-laden small intestinal submucosa enhances wound healing potential, Stem Cell Res. Ther. 11 (2020) 150, https://doi.org/10.1186/s13287-020-01662-2.
[9] M. Li, A. Zhang, J. Li, J. Zhou, Y. Zheng, C. Zhang, D. Xia, H. Mao, J. Zhao, Osteoblast/fibroblast coculture derived bioactive ECM with unique matrisome profile facilitates bone regeneration, Bioact. Mater. 5 (2020) 938–948, https://doi.org/10.1016/j.bioactmat.2020.06.017.
[10] B. Li, Y. Liu, Y. Zhou, P. You, M. Wang, L. Tang, Y. Deng, Developmentof a novel extracellular matrix membrane with an asymmetric structure for guided bone regeneration, Mater.,Lett. 274 (2020), 127926, https://doi.org/10.1016/j.matlet.2020.127926.
[11] M. Wang, B. Li, Y. Liu, L. Tang, Y. Zhang, Q. Xie, A novel bionic extracellular matrix polymer scaffold enhanced by calcium silicate for bone tissue engineering, ACS Omega 6 (2021) 35727–35737, https://doi.org/10.1021/acsomega.1c05623.
[12] S. Wang, W. Wu, Y. Liu, X. Wang, L. Tang, P. You, J. Han, B. Li, Y. Zhang, M. Wang, Bone augmentation of peri-implant dehiscence defects using multilaminated small intestinal submucosa as a barrier membrane: an experimental study in dogs, Biomed. Res. Int (2019) (2019), https://doi.org/10.1155/2019/8962730.
[13] W. Wu, B. Li, Y. Liu, X. Wang, L. Tang, Effect of multilaminate small intestinal submucosa as a barrier membrane on bone formation in a rabbit mandible defect model, Biomed. Res Int 2018 (2018) 3270293, https://doi.org/10.1155/2018/3270293.
[14] S.E. Kim, K. Park, Recent advances of biphasic calcium phosphate bioceramics for bone tissue regeneration, Adv. Exp. Med. Biol. 1250 (2020) 177–188, https://doi.org/10.1007/978-981-15-3262-7_12.
[15] H.D. Kim, S. Amirthalingam, S.L. Kim, S.S. Lee, J. Rangasamy, N.S. Hwang, Biomimetic materials and fabrication approaches for bone tissue engineering, Adv. Healthc. Mater. 6 (2017) 1700612, https://doi.org/10.1002/adhm.201700612.
[16] Y. Zhang, L. Xia, D. Zhai, M. Shi, Y. Luo, C. Feng, B. Fang, J. Yin, J. Chang, C. Wu, Mesoporous bioactive glass nanolayer-functionalized 3D-printed scaffolds for accelerating osteogenesis and angiogenesis, Nanoscale 7 (2015) 19207–19221, https://doi.org/10.1039/c5nr05421d.
[17] Q. Fu, M.N. Rahaman, H. Fu, X. Liu, Silicate, borosilicate, and borate bioactive glass scaffolds with controllable degradation rate for bone tissue engineering applications. I. Preparation and in vitro degradation, J. Biomed. Mater. Res. A 95 (2010) 164–171, https://doi.org/10.1002/jbm.a.32824.

[18] K. Zafar, S. Jamal, R. Ghafoor, Bio-active cements-mineral trioxide aggregate based calcium silicate materials: a narrative review, J. Pak. Med. Assoc. 70 (2020) 497–504, https://doi.org/10.5455/JPMA.16942.
[19] M.E. Frohbergh, A. Katsman, M.J. Mondrinos, C.T. Stabler, K.D. Hankenson, J. T. Oristaglio, P.I. Lelkes, Osseointegrative properties of electrospun hydroxyapatite-containing nanofibrous chitosan scaffolds, Tissue Eng. Part A 21 (2015) 970–981, https://doi.org/10.1089/ten.TEA.2013.0789.
[20] X. Meng, K. Gong, C. Sun, D. Liu, P. Du, D. Xu, Nonmineralized and mineralized silk fibroin/gelatin hybrid scaffolds: chacterization and cytocompatibility in vitro for bone-tissue engineering, J. Craniofacial Surg. 31 (2020) 416–419, https://doi.org/10.1097/SCS.0000000000006020.
[21] W. Jin, H. Wu, J. Shi, Z. Hu, Y. Zhou, Z. Chen, C. Shao, R. Tang, Z. Xie, Biomimetic mineralized collagen scaffolds enhancing odontogenic differentiation of hDPSCs and dentin regeneration through modulating mechanical microenvironment, in: Chemical Engineering Journal, 460, Lausanne, Switzerland, 1996, https://doi.org/10.1016/j.cej.2023.141800.
[22] J.H. Lee, J.H. Park, Y.R. Yun, J.H. Jang, E.J. Lee, W. Chrzanowski, I.B. Wall, H. W. Kim, Tethering bi-functional protein onto mineralized polymer scaffolds to regulate mesenchymal stem cell behaviors for bone regeneration, J. Mater. Chem. B 1 (2013) 2731–2741, http://doi.org.10.1039/c3tb00043e.
[23] X. Xie, W. Wang, J. Cheng, H. Liang, Z. Lin, T. Zhang, Y. Lu, Q. Li, Bilayer pifithrin-α loaded extracellular matrix/PLGA scaffolds for enhanced vascularized bone formation, Colloids Surf. B: Biointerfaces 190 (2020), 110903, https://doi.org/10.1016/j.colsurfb.2020.110903.
[24] S. Jin, F. Sun, Q. Zou, J. Huang, Y. Zuo, Y. Li, S. Wang, L. Cheng, Y. Man, F. Yang, J. Li, Fish collagen and hydroxyapatite reinforced poly(lactide-co-glycolide) fibrous membrane for guided bone regeneration, Biomacromolecules 20 (2019) 2058–2067, hhttp://doi.org/10.1021/acs.biomac.9b00267.
[25] H. Tebyanian, M.H. Norahan, H. Eyni, M. Movahedin, S.J. Mortazavi, A. Karami, M.R. Nourani, N. Baheiraei, Effects of collagen/beta-tricalcium phosphate bone graft to regenerate bone in critically sized rabbit calvarial defects, J. Appl. Biomater. Funct. Mater. 17 (2019) 585952650, https://doi.org/10.1177/2280800018820490.
[26] W. Cui, L. Yang, I. Ullah, K. Yu, Z. Zhao, X. Gao, T. Liu, M. Liu, P. Li, J. Wang, X. Guo, Biomimetic porous scaffolds containing decellularized small intestinal submucosa and Sr(2+)/Fe(3+)co-doped hydroxyapatite accelerate angiogenesis/osteogenesis for bone regeneration, Biomed. Mater. 17 (2022), https://doi.org/10.1088/1748-605X/ac4b45.
[27] Y. Liu, N. Li, Y.P. Qi, L. Dai, T.E. Bryan, J. Mao, D.H. Pashley, F.R. Tay, Intrafibrillar collagen mineralization produced by biomimetic hierarchical nanoapatite assembly, Adv. Mater. 23 (2011) 975–980, https://doi.org/10.1002/adma.201003882.
[28] H. Liu, M. Lin, X. Liu, Y. Zhang, Y. Luo, Y. Pang, H. Chen, D. Zhu, X. Zhong, S. Ma, Y. Zhao, Q. Yang, X. Zhang, Doping bioactive elements into a collagen scaffold based on synchronous self-assembly/mineralization for bone tissue engineering, Bioact. Mater. 5 (2020) 844–858, https://doi.org/10.1016/j.bioactmat.2020.06.005.
[29] R. Chen, R. Jin, X. Li, X. Fang, D. Yuan, Z. Chen, S. Yao, R. Tang, Z. Chen, Biomimetic remineralization of artificial caries dentin lesion using Ca/P-PILP, Dent. Mater. 36 (2020) 1397–1406, http:///doi.org/10.1016/j.dental.2020.08.017.
[30] B. Li, M. Wang, Y. Liu, Y. Zhou, L. Tang, P. You, Y. Deng, Independent effects of structural optimization and resveratrol functionalization on extracellular matrix scaffolds for bone regeneration, Colloids Surf. B: Biointerfaces (2022), 112370, https://doi.org/10.1016/j.colsurfb.2022.112370.
[31] S. Yao, X. Lin, Y. Xu, Y. Chen, P. Qiu, C. Shao, B. Jin, Z. Mu, N.A.J.M. Sommerdijk, R. Tang, Osteoporotic bone recovery by a highly bone-inductive calcium phosphate polymer-induced liquid-precursor, Adv. Sci. 6 (2019) 1900683, http://doi.org/10.1002.advs.201900683.
[32] H.X. Wang, Z.Y. Li, Z.K. Guo, Z.K. Guo, Easily-handled method to isolate mesenchymal stem cells from coagulated human bone marrow samples, World J. Stem Cells 7 (2015) 1137–1144, https://doi.org/10.4252/wjsc.v7.i8.1137.
[33] Y. Huang, D. Seitz, F. Konig, P.E. Muller, V. Jansson, R.M. Klar, Induction of articular chondrogenesis by chitosan/hyaluronic-acid-based biomimetic matrices using human adipose-derived stem cells, Int. J. Mol. Sci. 20 (2019), https://doi.org/10.3390/ijms20184487.
[34] K.J. Livak, T.D. Schmittgen, Analysis of relative gene expression data using real-time quantitative PCR and the 2−ΔΔCT method, Methods 25 (2001) 402–408, https://doi.org/10.1006/meth.2001.1262.
[35] N. Abbasi, S. Hamlet, R.M. Love, N. Nguyen, Porous scaffolds for bone regeneration, J. Sci.: Adv. Mater. Devices 5 (2020) 1–9, https://doi.org/10.1016/j.jsamd.2020.01.007.
[36] S.W. Choi, Y. Zhang, Y. Xia, Three-dimensional scaffolds for tissue engineering: the importance of uniformity in pore size and structure, Langmuir 26 (2010) 19001–19006, https://doi.org/10.1021/la104206h.
[37] N. Abbasi, A. Abdal-Hay, S. Hamlet, E. Graham, S. Ivanovski, Effects of gradient and offset architectures on the mechanical and biological propertiesof 3-D melt electrowritten (MEW) Scaffolds, ACS Biomater. Sci. Eng. 5 (2019) 3448–3461, https://doi.org/10.1021/acsbiomaterials.8b01456.
[38] J.H. Wen, L.G. Vincent, A. Fuhrmann, Y.S. Choi, K.C. Hribar, H. Taylor-Weiner, S. Chen, A.J. Engler, Interplay of matrix stiffness and protein tethering in stem cell differentiation, Nat. Mater. 13 (2014) 979–987, https://doi.org/10.1038/nmat4051.
[39] J.D. Humphrey, E.R. Dufresne, M.A. Schwartz, Mechanotransduction and extracellular matrix homeostasis, Nat. Rev. Mol. Cell Biol. 15 (2014) 802–812, https://doi.org/10.1038/nrm3896.
[40] R.G. Wells, The role of matrix stiffness in regulating cell behavior, Hepatol. (Baltim., Md.) 47 (2008) 1394–1400, http://doi.org/10.1002hep.22193.
[41] K. Liu, M. Wiendels, H. Yuan, C. Ruan, P. Kouwer, Cell-matrix reciprocity in 3D culture models with nonlinear elasticity, Bioact. Mater. 9 (2022) 316–331, https://doi.org/10.1016/j.bioactmat.2021.08.002.
[42] A. El-Fiqi, J.H. Kim, H.W. Kim, Novel bone-mimetic nanohydroxyapatite/collagen porous scaffolds biomimetically mineralized from surface silanized mesoporous nanobioglass /collagen hybrid scaffold: Physicochemical, mechanical and in vivo evaluations, Mater. Sci. Eng. C. Mater. Biol. Appl. 110 (2020), 110660 http://doi.org/10.10 16/j.msec.2020.110660.
[43] Y. Fu, S. Liu, S.J. Cui, X.X. Kou, X.D. Wang, X.M. Liu, Y. Sun, G.N. Wang, Y. Liu, Y. H. Zhou, Surface chemistry of nanoscale mineralized collagen regulates periodontal ligament stem cell fate, ACS Appl. Mater. Interfaces 8 (2016) 15958–15966, https://doi.org/10.1021/acsami.6b04951.
[44] J. Wang, Q. Liu, Z. Guo, H. Pan, Z. Liu, R. Tang, Progress on biomimetic mineralization and materials for hard tissue regeneration, ACS Biomater. Sci. Eng. (2021), https://doi.org/10.1021/acsbiomaterials.1c01070.
[45] J. Moradian-Oldak, A. George, Biomineralization of enamel and dentin mediated by matrix proteins, J. Dent. Res. 100 (2021) 1020–1029, http://doi.org/10.1177/00 220345211018405.
[46] Q. Yao, Y.W. Zheng, Q.H. Lan, L. Kou, H.L. Xu, Y.Z. Zhao, Recent development and biomedical applications of decellularized extracellular matrix biomaterials, Mater. Sci. Eng. C. Mater. Biol. Appl. 104 (2019), 109942, https://doi.org/10.1016/j.msec.2019.109942.
[47] G.C. Reilly, A.J. Engler, Intrinsic extracellular matrix properties regulate stem cell differentiation, J. Biomech. 43 (2010) 55–62, https://doi.org/10.1016/j.jbiomech.2009.09.009.
[48] A.B.S.H. Zetao Chen, Tuning chemistry and topography of nanoengineered surfaces to manipulate immune response for bone regeneration applications, ACS Nano 5 (2017) 4494–4506, https://doi.org/10.1021/acsnano.9b01008.
[49] J. De Waele, K. Reekmans, J. Daans, H. Goossens, Z. Berneman, P. Ponsaerts, 3D culture of murine neural stem cells on decellularized mouse brain sections, Biomaterials 41 (2015) 122–131, https://doi.org/10.1016/j.biomaterials.2014.11.025.
[50] V. Navarro-Tableros, S.M. Herrera, F. Figliolini, R. Romagnoli, C. Tetta, G. Camussi, Recellularization of rat liver scaffolds by human liver stem cells, Tissue Eng. Part A 21 (2015) 1929–1939, https://doi.org/10.1089/ten.TEA.2014.0573.
[51] T. Sun, C. Meng, Q. Ding, K. Yu, X. Zhang, W. Zhang, W. Tian, Q. Zhang, X. Guo, B. Wu, Z. Xiong, In situ bone regeneration with sequential delivery of aptamer and BMP2 from an ECM-based scaffold fabricated by cryogenic free-form extrusion, Bioact. Mater. 6 (2021) 4163–4175, https://doi.org/10.1016/j.bioactmat.2021.04.013.
[52] T. Sun, S. Yao, M. Liu, Y. Yang, Y. Ji, W. Cui, Y. Qu, X. Guo, Composite Scaffolds of mineralized natural extracellular matrix on true bone ceramicinduce bone regeneration through Smad1/5/8 and ERK1/2 pathways, Tissue Eng. Part A 24 (2018) 502–515, https://doi.org/10.1089/ten.TEA.2017.0179.
[53] M. Shie, S. Ding, H. Chang, The role of silicon in osteoblast – like cell proliferation and apoptosis, Acta Biomater. 7 (2011) 2604–2614, https://doi.org/10.1016/j.actbio.2011.02.023.